



Ultrafast element-specific magnetization dynamics of complex magnetic materials on a table-top

Stefan Mathias^{a,b,*}, Chan La-o-vorakiat^b, Justin M. Shaw^d, Emrah Turgut^b, Patrik Grychtol^{b,c}, Roman Adam^c, Dennis Rudolf^c, Hans T. Nembach^d, Thomas J. Silva^d, Martin Aeschlimann^a, Claus M. Schneider^c, Henry C. Kapteyn^b, Margaret M. Murnane^b

^a University of Kaiserslautern and Research Center OPTIMAS, 67663 Kaiserslautern, Germany

^b Department of Physics and JILA, University of Colorado and NIST, Boulder, CO, 80309 USA

^c Peter Grünberg Institut PGI-6 & JARA-FIT, Research Centre Jülich, 52425 Jülich, Germany

^d Electromagnetics Division, National Institute of Standards and Technology, Boulder, CO, 80305 USA

ARTICLE INFO

Article history:

Available online 21 December 2012

Keywords:

Magnetism
Ultrafast
Femtosecond
Dynamics
High-harmonic generation
Material science
X-ray

ABSTRACT

We review recent progress in femtosecond magnetization dynamics probed by extreme ultraviolet pulses from high-harmonic generation. In a transverse magneto-optical Kerr geometry, we established an ultrafast, element-specific experimental capability – on a table-top – for the measurement of magnetization dynamics in complex multi-sublattice magnets and multilayer magnetic structures. We show that this newly introduced technique is an artifact-free magnetic sensor, with only negligible non-magnetic (optical) contributions from the transient variation of the refractive index due to the presence of a non equilibrium hot-electron distribution. We then use these new experimental capabilities of ultrahigh time-resolution, combined with element-specific simultaneous probing, to disentangle important microscopic processes that drive magnetization dynamics on femtosecond timescales. We elucidate the role of exchange interaction on magnetization dynamics in strongly exchange-coupled alloys, and the role of photo-induced superdiffusive spin currents in magnetic multilayer stacks.

© 2012 Elsevier B.V. All rights reserved.

1. Introduction

Femtomagnetism, which is the manipulation of magnetic order on femtosecond timescales by ultrashort laser pulses, was first observed by Eric Beaurepaire et al. in 1996 [1]. Since then, femtomagnetism has become a challenging research topic of increasing interest because of its importance for uncovering fundamental new science and for technological applications. Typically, experiments that study femtomagnetism are carried out in a pump-probe geometry. An intense femtosecond laser pulse first excites a magnetic system, and the resulting ultrafast changes of the magnetization are then probed magneto-optically and by spin-resolved photoemission. The dynamical response of the magnetic material to the excitation by an ultrashort laser pulse is governed by non equilibrium interactions between photons, electrons, spins, and phonons (see Fig. 1). Despite nearly two decades of research, the fundamental microscopic processes involved in femtomagnetism are not well understood, and indeed are still a topic of intense debate [2–13]. One of the key challenges is to carefully disentangle

the various dynamical processes shown in Fig. 1 to establish how they contribute to the behavior of a complex magnetic system far from equilibrium. This quest demands the development of new experimental capabilities. For example, the investigation of coherent magnetization dynamics [7,14] in the time domain requires extremely high time-resolution (<20 fs), while the influence of exchange-coupling on magnetization dynamics [15] requires element-specificity. Finally, to capture superdiffusive spin-transport in magnetic multilayer stacks [16], we require ultrafast element-specific, layer-selective probes of the magnetization state [16–18].

The ideal experimental technique would therefore combine sensitivity to the magnetization state with femtosecond-to-attosecond time-resolution, be able to distinguish the signal from different elements in an alloy or multilayer system, and be able to image with nanometer spatial resolution. This is a challenging task, but one that can be achieved by use of femtosecond slicing technique [17,18], the newly developed large-scale X-ray free-electron lasers (XFELs) [19,20], and table-top-scale high-harmonic generation (HHG) light sources [15,16,21–23]. Comparing magnetic dynamics probed by HHG and femtosecond slicing sources or XFELs, it is becoming clear that all of these techniques are complementary and have unique advantages. High harmonic probes at the M absorption edges have the advantages of probing the magnetic state of multiple

* Corresponding author at: University of Kaiserslautern and Research Center OPTIMAS, 67663 Kaiserslautern, Germany.

E-mail address: smathias@physik.uni-kl.de (S. Mathias).

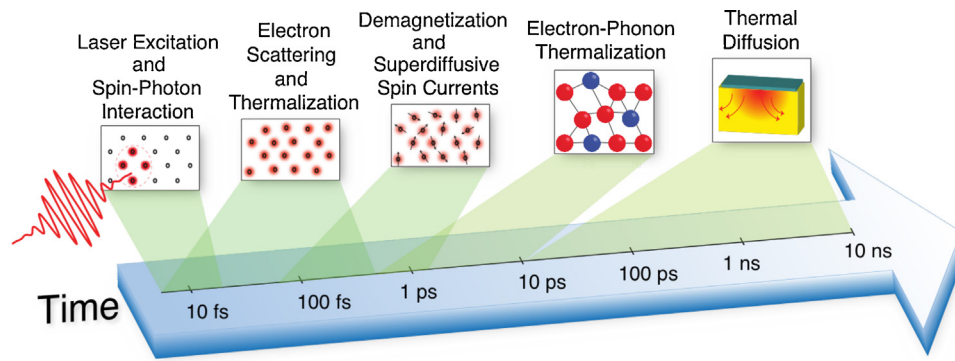


Fig. 1. Adapted from [15]. Schematic timeline of ultrafast photon–electron–spin–lattice interactions after an ultrafast laser excitation. During the ultrafast excitation of the electron system by a femtosecond laser pulse, ultrafast spin–photon interaction can be a source of magnetization dynamics [6,7,14,29]. On a longer femtosecond timescale, various scattering processes between electrons, phonons, and magnons, as well as superdiffusive spin-currents [8,16,30,31] determine the dynamic response of the material. The strongly excited electron system thermalizes by predominantly electron–electron scattering to a Fermi–Dirac distribution. Spin-flip electron–electron [5,11], electron–phonon [3,4,9–11,32], and electron–magnon [10,33] scattering processes, together with superdiffusive spin currents [8,16,30,31] mediate the magnetization dynamics. Electron–phonon scattering transfers the energy from the excited electron gas to the lattice, and thermal equilibrium is typically reached on picosecond timescales. Finally, on nanosecond timescales, the material cools by thermal diffusion. The different contributions of the above-mentioned processes to the ultrafast magnetic dynamics are widely debated.

elements simultaneously, allowing the fastest coupled dynamics to be uncovered with very high precision. This source is also compact and accessible. Synchrotrons and XFELs can probe dynamics at the higher-energy L-shell absorption edges, allowing spin and orbital contributions to be extracted, and enabling higher spatial resolution imaging.

In this paper, we review how HHG light sources can uncover the fastest dynamics in femtomagnetism [15,16,21,22]. HHG is an extremely nonlinear process that produces coherent short-wavelength beams with the shortest pulse durations in the few femtosecond to attosecond regime demonstrated to date for any light source [24–28]. Bright harmonic beams now span from 10 eV to greater than 2 keV [28] while retaining the polarization and coherence properties of the driving laser under phase-matched generation conditions. We show that table-top HHG sources are ideal probes of femtomagnetism because of their artifact-free sensitivity to the magnetization [22], femtosecond time resolution, and element-specificity at multiple sites simultaneously [21]. These unique new experimental capabilities make it possible to solve long-standing problems in femtomagnetism [16], and also enable more complex and technologically relevant magnetic materials to be studied [15]. HHG has already been used to capture the fastest magnetization dynamics in elemental materials, complex magnetic alloys, and multilayer systems, thereby elucidating the role of exchange interaction and superdiffusive spin currents in ultrafast magnetization dynamics.

2. The transverse magneto-optical Kerr effect in the XUV regime

Femtosecond extreme ultraviolet (XUV) pulses from HHG are produced by focusing 90% of an amplified, femtosecond laser pulse (780 nm wavelength, 2–3 kHz repetition rate, 1.5–2.5 mJ per pulse) into a capillary-waveguide filled with Ne (Fig. 2). For high-efficient phase-matched high-harmonic up-conversion, we optimize the gas pressure in the waveguide at values around 800 Torr [25,27]. A broad range of harmonics spanning photon energies from 35 eV to 72 eV are emitted simultaneously. The cutoff at 72 eV is due to the absorption edge of the Al filters that are used to block the laser light that co-propagates with the HHG beam. The duration of the high-harmonic XUV pulses is less than 10 fs [34].

We use a transversal magneto-optical Kerr (T-MOKE) geometry to probe the magnetic state of our samples (Fig. 2, inset), where, for a single magnetic layer, the polarization-dependent reflected

intensity of the XUV beam for p-polarized incident light is [35,36]:

$$I_{\pm}^p = I_0 \left| \frac{n \cos \theta_i - \cos \theta_t}{n \cos \theta_i + \cos \theta_t} \pm \frac{2 \sin \theta_i \cos \theta_i}{n^2 (n \cos \theta_i + \cos \theta_t)^2} \epsilon_{xy} \right|^2 \quad (1)$$

and for s-polarized incident light is

$$I^s = I_0 \left| \frac{\cos \theta_i - n \cos \theta_t}{\cos \theta_i + n \cos \theta_t} \right|^2 \quad (2)$$

where I_0 is the incident beam intensity, n the refractive index of the material, θ_i the angle of incidence, $\theta_t = \sin^{-1}(\sin \theta_i/n)$ the refractive angle, the plus-minus sign depends on the direction of the in-plane magnetization, and ϵ_{xy} the magnetization-dependent off-diagonal element of the dielectric tensor. For p-polarized light, the first term inside the absolute square of Eq. (1) is the non-magnetic Fresnel coefficient for the sample reflectivity. The dependence of the reflectivity on the magnetic state is contained in the second term

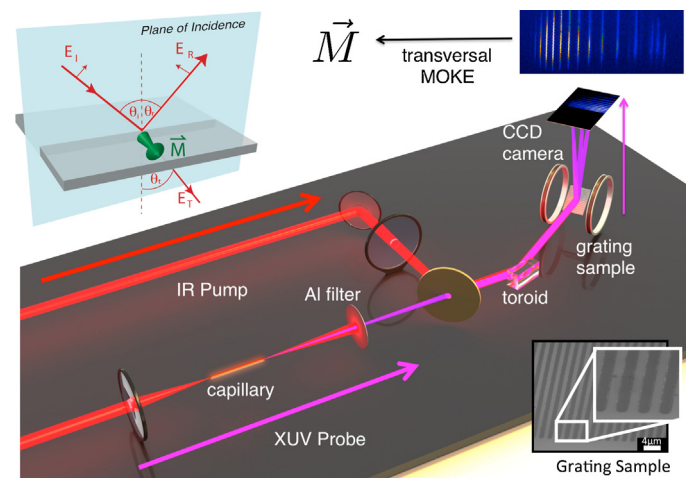


Fig. 2. Adapted from [15]. Schematic of the experiment. Ultrafast XUV pulses are reflected from a magnetic sample with a grating on top, which spatially separates the harmonics to form a spectrum on a CCD camera. The reflected HHG intensity at the shallow-core absorption edges depends on the magnetization transverse to the optical plane of incidence (T-MOKE, see inset) that is periodically reversed by transverse-mounted Helmholtz coils. Exciting the sample with an ultrashort laser pulse (red) initiates the magnetization dynamics. (For interpretation of the references to color in the artwork, the reader is referred to the web version of the article.)

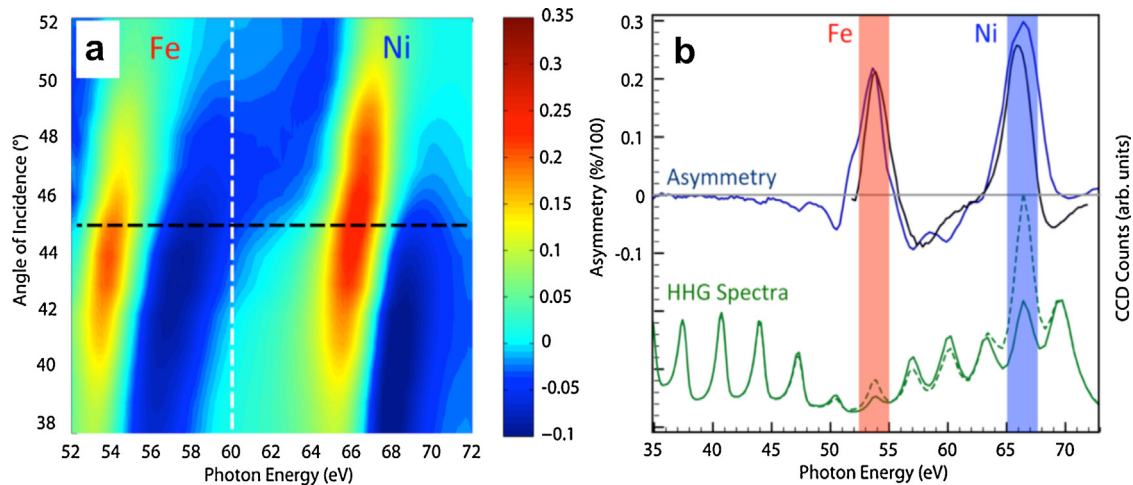


Fig. 3. From [15]. XUV spectra and magnetic asymmetry. (a) Magnitude of the asymmetry from a Permalloy sample, coded in color, as a function of photon energy and angle of incidence, measured with synchrotron radiation. The asymmetry signal of Fe (≈ 54 eV) is clearly separated from Ni (≈ 67 eV). (b) HHG XUV spectra reflected from a Permalloy grating sample at an angle of incidence of 45° , shown as green solid and dotted lines for the two different magnetization directions. The blue line is the asymmetry from the HHG spectra, and the black line the asymmetry from synchrotron data that corresponds to the spectral cut shown as a black dashed line in (a).

via the dielectric magneto-optical constant ϵ_{xy} , which is in first approximation linearly proportional to the magnetization component perpendicular to the plane of incidence. We consider the change of the reflectivity only up to the first order in the magneto-optical constant, since the magneto-optical constants are usually small numbers ($\sim 10^{-3}$) [35,36]. Note that Eq. (2) shows that the sample reflectivity for s-polarized incident light is always independent of the magnetization.

The magnetic signal is extracted by first measuring the reflected light for both magnetization directions (I_+^p and I_-^p , respectively), and then calculating the magnetic asymmetry parameter (A) given by:

$$\begin{aligned}
 A &= \frac{I_+^p - I_-^p}{I_+^p + I_-^p} \cong 2 \operatorname{Re} \left[\frac{\sin(2\theta_i) \epsilon_{xy}}{n^4 \cos^2 \theta_i - n^2 + \sin^2 \theta_i} \right] \\
 &= 2 \operatorname{Re} \left[\frac{\sin(2\theta_i) \epsilon_{xy}}{(n^2 - 1)[n^2 - \sin^2 \theta_i(n^2 + 1)]} \right] \\
 &\cong \frac{\sin(2\theta_i)}{1 - 2\cos^2 \theta_i} \left(\frac{\delta \operatorname{Re}[\epsilon_{xy}] + \beta \operatorname{Im}[\epsilon_{xy}]}{\delta^2 + \beta^2} \right) \quad (3)
 \end{aligned}$$

here, we assume that the Fresnel coefficient is large compared to the magneto-optical term. In Eq. (3), we substitute the complex representation of the refractive index $n = 1 - \delta + i\beta$, where δ and β are small numbers. The most critical property of the calculated asymmetry (A) is that the asymmetry is also a function of the refractive index (n). This shows that a photo-induced index change in the ultrafast experiment will introduce an artifact to the experimentally determined magnetic dynamics. Fortunately, in Section 3 we can show that in the XUV regime, this artifact is negligible compared to the T-MOKE magnetic signal.

In order to distinguish the magnetic dynamics of different elements in alloys and multilayer structures, we need to measure the reflectivity as a function of photon energy near the various $M_{2,3}$ shell absorption edges of 3d ferromagnets, where the asymmetry signal is maximum. At these atomic absorption edges, the off-diagonal element of the dielectric tensor ϵ_{xy} is resonantly enhanced and the magnetic asymmetry is therewith increased from less than one percent in the visible spectral range [37] up to tens of percent in the XUV range [38] (see Fig. 3). This increase of ϵ_{xy} over its analog in the visible spectral range is due to the large spin-orbit and exchange splitting of the $3p$ shallow core states [39]. Note also that the measured T-MOKE asymmetry is

wavelength-dependent through $n(\omega)$ and the off-diagonal magnetic component of the dielectric tensor $\epsilon_{xy}(\omega)$ [40,41]. Therefore, even the individual magnetic signal of a single element, which extends over several eV in the XUV range, should be measured as a function of photon energy. We therefore incorporate a spectrometer into the samples by fabricating the samples into diffraction gratings (or overlaying a diffracting structure on the sample: see bottom right of Fig. 2). The reflected HHG spectrum from the sample is then captured by an X-ray CCD camera placed at a 45° angle-of-incidence geometry to maximize the asymmetry (Brewster's angle, see second line of Eq. (3) and Fig. 2). The femtosecond pump beam that is used to initiate the magnetization dynamics is blocked from the CCD camera by use of two 200 nm Al filters.

Fig. 3 shows the magnetic asymmetry for a $\text{Ni}_{80}\text{Fe}_{20}$ alloy sample (Permalloy), which was measured by use of T-MOKE with light from a synchrotron (3a) and a HHG light source (3b). The magnetic asymmetry (color-coded in Fig. 3a) is measured as a function of sample angle-of-incidence and XUV energy. Fe and Ni can be distinguished by their energy-dependent magnetic asymmetry peaks that are approximately left and right of the white dashed line for Fe and Ni, respectively [38,42,43]. Note that the measured signal corresponds to excitations of localized M-shell electrons into unoccupied states above the Fermi energy. Therefore, HHG XUV T-MOKE probes magnetic moments in the vicinity of each atom of the specific element under investigation, and in this sense provides a localized probe of magnetic moments.

As explained above and from Eq. (3), the largest magnetic asymmetry occurs at an angle of incidence of 45° (black line in Fig. 3a), which is therefore the geometry chosen for the HHG probe setup. Fig. 3b compares the measured magnetic asymmetries for both synchrotron and HHG light at a 45° angle-of-incidence. Integration times for a reasonable asymmetry spectrum as shown in Fig. 3b are around 100 s (50 s for each magnetization direction). The MOKE spectra from synchrotron and XUV T-MOKE are in good agreement with each other. Although the high-harmonic spectrum exhibits the expected odd-harmonic structure, for sub-10 fs XUV pulses, as is the case in all our presented experiments, the bandwidth of each harmonic is broad, with real spectral content between the peaks. In other words, there is some spectral overlap between the different harmonic orders. Therefore, for our experiment, where we measure the normalized magnetic asymmetry, we essentially have an ultrafast XUV white light source available, which allows us to follow the dynamics of different elemental constituents in alloys

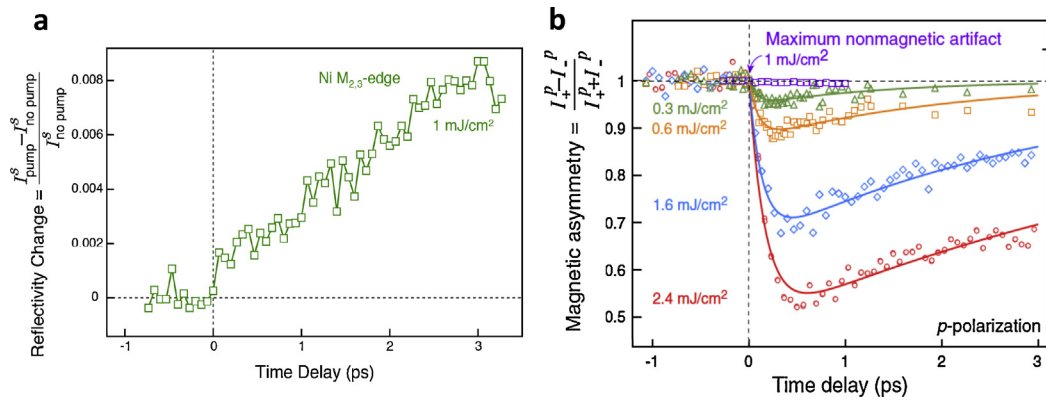


Fig. 4. From [22]. Estimation of the maximum non-magnetic artifact with XUV T-MOKE. (a) Nonmagnetic reflectivity for a pump fluence of 1 mJ/cm² (780 nm, 25 fs), measured by the use of an s-polarized XUV probe beam at the Ni M_{2,3} absorption edge (to see the long-time behavior, see Ref. [22]). (b) The maximum non-magnetic artifact is inferred from this resonant reflectivity measurement and plotted together with fluence dependent demagnetization data in Ni. The potential artifact of 0.2% within the first 300 fs is about 2 orders of magnitude lower than the demagnetization amplitude of 20% measured with the same pump fluence.

and multilayers. This is a huge advantage for time-resolved experiments because we can very accurately and simultaneously measure correlated dynamics of individual elements in complex magnetic materials and structures.

3. Magnetism vs. optics: an artifact-free probe of ultrafast magnetism

For all time-resolved magneto-optical Kerr experiments performed to date, whether with visible or soft X-ray probes, there has been a long-standing debate about the potential presence of nonmagnetic artifacts in the magnetic signal, which can be induced by the femtosecond pump pulse that initiates the dynamics [44–50]. For our newly developed XUV T-MOKE technique, we therefore did a detailed investigation to assess the contribution of any non-magnetic artifacts in our magnetic signal. Through careful experiments that separated the electronic and magnetic contributions, we could show that T-MOKE in the XUV is highly sensitive to spin-dynamics with negligible non-magnetic contributions [22].

Non-magnetic artifacts in time-resolved pump-probe experiments can be introduced by so-called state-blocking and by the generation of non equilibrium electron distributions. State blocking refers to the saturation of an optical transition by the pump-pulse, and can always be suppressed or even avoided by use of different pump and probe wavelengths, i.e., pumping and probing different optical transitions in the material. In addition, pump-induced non-equilibrium electron distributions strongly and transiently modify the occupation density of the valence states just around the Fermi level. However, most of these effects are invariant under magnetization reversal and thus can be eliminated by measuring the magneto-optical contrast for both magnetization directions. Unfortunately, the value of the magnetic asymmetry can still be influenced by the transient change of the refractive index after optical excitation (see Eq. (3)).

Experimentally, we can isolate the non-magnetic contribution to the asymmetry signal by measuring the pump-induced transient refractive index change, and by using Eq. (3) to calculate upper limits of the resulting artificial (non-magnetic) contribution to the asymmetry parameter A . Fig. 4a shows the measured transient reflectivity in resonance with the Ni M_{2,3} absorption edge at 68 eV after excitation of the sample with a typical fluence of 1 mJ/cm². Since s-polarized probe light is insensitive to magnetic contributions, the fast change of the reflectivity must result only from the transient variation of the refractive index. Note that the refractive index is the only parameter in Eq. (2). Based on this measured transient change in the s-polarization reflectivity, the

transient modification of the refractive index can be estimated by calculating the upper bounds for the change of the real and imaginary components of the refractive index $n = 1 - \delta + i\beta$. The reflectivity at resonance changes by about 0.2% during the first 300 fs (the relevant time scale for both demagnetization and hot-electron dynamics, see Fig. 4), which corresponds to a δ or β change by no more than 3% or 0.1%, respectively (from a numerical solution of Eq. (2)). Using Eq. (3), we calculate the expected transient change in the asymmetry parameter and see that the measured time-dependent magnetic signal can include an artifact of less than $\sim 0.2\%$ during the first 300 fs of the demagnetization dynamics (Fig. 4b). This optically induced artifact is *two orders of magnitude smaller* than the observed demagnetization amplitude of about 20%. Time-resolved XUV T-MOKE therefore represents an ideal experimental capability to measure pure magnetization-dynamics in complex materials.

4. Ultrafast magnetism in complex magnetic materials: from single elemental materials to alloys and multilayer structures

Having thoroughly characterized the HHG XUV T-MOKE technique [21,22], we turn now to the investigation of ultrafast magnetic dynamics in complex materials (Fig. 5). The two ferromagnetic elements Ni and Fe are investigated under changing environmental conditions. We first start with elemental Ni and Fe in order to compare with state-of-the-art experiments, i.e., the “usual” demagnetization dynamics. We then successively increase the complexity of the material system by alloying Ni and Fe in Permalloy (Ni₈₀Fe₂₀). The magnetic moments of Ni and Fe in Permalloy are strongly exchange coupled, so that one might assume identical ultrafast magnetization dynamics for the two constituting elements. However, we show that on ultrafast timescales, the dynamics of Ni and Fe in Permalloy are distinct and, moreover, are determined by the strength of the exchange coupling. We verify this result in another experimental step by introducing non-magnetic Cu atoms into the Permalloy. This weakens the interatomic exchange coupling in the Ni–Fe–Cu alloy, so that even more distinct demagnetization dynamics of the constituents Ni and Fe are found [15]. Finally, we move from alloys to multilayer structures, where we couple elemental Ni and Fe magnetic moments in magnetic–nonmagnetic–magnetic trilayer stacks. In the trilayer stack, however, interlayer exchange coupling is so weak that we cannot expect to see any influence of the interlayer coupling on the magnetic dynamics on ultrafast timescales. Even more surprising is that in the trilayer stack, the elements Ni and Fe do not react like elemental materials on ultrafast timescales, but rather show a

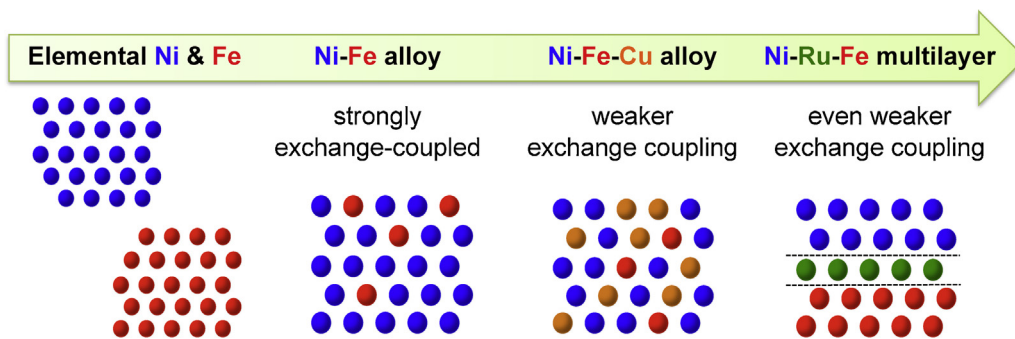


Fig. 5. The two ferromagnetic materials Ni and Fe are investigated under changing interatomic and interlayer magnetic coupling conditions. We first start with elemental Ni and Fe and then successively increase the complexity of the material system, moving to Permalloy ($\text{Ni}_{80}\text{Fe}_{20}$), Permalloy alloyed with Cu, and finally a Ni–Ru–Fe trilayer stack. Such a controlled modification of the magnetic material system enables us to disentangle the role of exchange coupling and superdiffusive spin currents in femtosecond magnetization dynamics.

strong dependence on the relative orientation (parallel vs. antiparallel). We show that our results in the magnetic multilayer stack can be explained by taking photo-induced superdiffusive spin-currents into account [16].

Fig. 6a shows a simultaneous measurement of the magnetization dynamics of elemental Ni and Fe for an interleaved stripe sample of both elements. After excitation with a laser fluence of $\approx 2 \text{ mJ}/\text{cm}^2$, Ni and Fe show the “usual” demagnetization behavior that has been studied over almost the past two decades. The magnetization decreases rapidly and is quenched by about 19% for Fe and 45% for Ni at the same pump fluence. Using a double exponential fitting function given by $m(t) = 1 - \Delta m [1 - \exp(-t/\tau_m)] \exp(-t/\tau_r)$, we can extract the demagnetization times of $\tau_m = 98 \pm 26 \text{ fs}$ for Fe and $157 \pm 9 \text{ fs}$ for Ni, in agreement with earlier studies for similar pump fluencies [4,33].

Now, we move from single-species ferromagnets to the more complex binary ferromagnet Permalloy (Py), where the constituents Fe and Ni are miscible and strongly exchange-coupled. Therefore, we might expect identical demagnetization dynamics for the two elements, particularly for a completely delocalized, itinerant spin-polarized band structure. Indeed, Fig. 6b shows that the magnetization decreases rapidly for both elements in Permalloy to a common minimum of about 70% of the total magnetization. However, a closer look at the short-timescale data shows that in all our measurements, the demagnetization of Fe precedes that of Ni by approximately 10–20 fs.

The degree to which magnetization dynamics can be different for Ni and Fe in Permalloy surely must depend on the strength of the Ni–Fe interatomic exchange coupling: the weaker the Ni–Fe exchange coupling, the more the dynamics can differ without incurring too large of an energy cost. We therefore repeated our measurement for the Permalloy alloyed with Cu, $\text{Py}_{60}\text{Cu}_{40}$, where the volume-averaged exchange parameter is reduced through the reduction of the number of ferromagnetic nearest-neighbor atoms [15]. Fig. 6c shows a plot of the magnetization dynamics of Permalloy–Cu. There is a clear demagnetization delay of approximately 76 fs for Ni relative to Fe, as indicated by the arrows. Our experiment thus provides the first direct observation of the influence of exchange coupling on femtosecond magnetization dynamics. As such, our data help to elucidate the microscopic role of exchange interaction in femtomagnetism, a contribution to the ultrafast dynamics that we assume will be of general importance in complex magnetic compounds and alloyed materials. We note that without the ability to measure magnetization dynamics at the elemental Fe and Ni sites simultaneously that uncovered delays of 10–80 fs (depending on the alloy), this experiment would likely not have been possible.

Finally, we further modified the material system, and weakened the exchange coupling between the elements Ni and Fe, by fabricating an interlayer exchange coupled ferromagnet–paramagnet–ferromagnet trilayer stack. Because of the extremely weak interlayer exchange coupling in the multilayer stack compared to the interatomic exchange coupling in the Permalloy, we might not expect any influence of the interlayer coupling on the femtosecond magnetization dynamics of Ni and Fe. Fig. 6d shows the ultrafast demagnetization dynamics of Ni and Fe in an antiferromagnetically coupled Ni(5 nm)/Ru(1.5 nm)/Fe(4 nm) trilayer, at a laser fluence of about $2 \text{ mJ}/\text{cm}^2$. In comparison to the measurement of elemental Ni and Fe (Fig. 6a), the magnetization quenching of Ni is stronger than in the elemental case, while the magnetization quenching of Fe is comparable, respectively. From a qualitative point of view, however, we would expect less quenching of the Fe magnetization at comparable fluence, because the Fe in the multilayer stack is buried below a 3 nm Al-capping layer, a 5 nm Ni layer, and a 1.5 nm Ru layer. The Ni quenching, on the other hand, should be comparable to the elemental measurement, but is even larger in the multilayer stack. Note that for elemental Ni, a change in the magnetization quenching from 40% to 60% would require an increase in pump fluence from $\approx 2 \text{ mJ}/\text{cm}^2$ to $\approx 3 \text{ mJ}/\text{cm}^2$ [4,22]. We therefore exclude minor variations in fluence between the two measurements (Fig. 6a vs. d) as the source of the strongly disproportionate dynamics.

For the trilayer system, we find instead that the magnetization dynamics are consistent if transport of laser-excited spin-majority spins [8,31,52,53] from the top Ni layer to the buried Fe layer is taken into account in addition to the optical excitation [16]. Since the inelastic mean free path for the majority spins in Ni with energies of a few eV above the Fermi level is higher than for the minority spins [54], superdiffusive transport of majority spins from Ni into the buried Fe layer generate magnetization orientation-dependent (parallel vs. antiparallel) ultrafast spin dynamics (The spin-current is initially ballistic on timescales of 5 fs to 10 fs, after which it becomes diffusive as the electrons thermalize [8,31]). First, majority spins superdiffusing out of the Ni top layer seem to add to the optically induced demagnetization dynamics in Ni (c.f. Fig. 6a). Then, in the case of antiparallel magnetization-alignment of the Ni and Fe layers, the Ni majority spins enter the Fe layer and drive the demagnetization process in Fe by transiently increasing the number of Fe minority spins to just above the Fermi level. Note here that the Fe layer is intrinsically less sensitive to the direct optical excitation in comparison to Ni [15], and that the Fe layer is moreover buried below Al–Ni–Ru layers. Therefore, superdiffusing majority spins from the Ni layer present the dominant process for the observed magnetization dynamics in the Fe layer. In consequence, the mechanism of superdiffusive spin transport

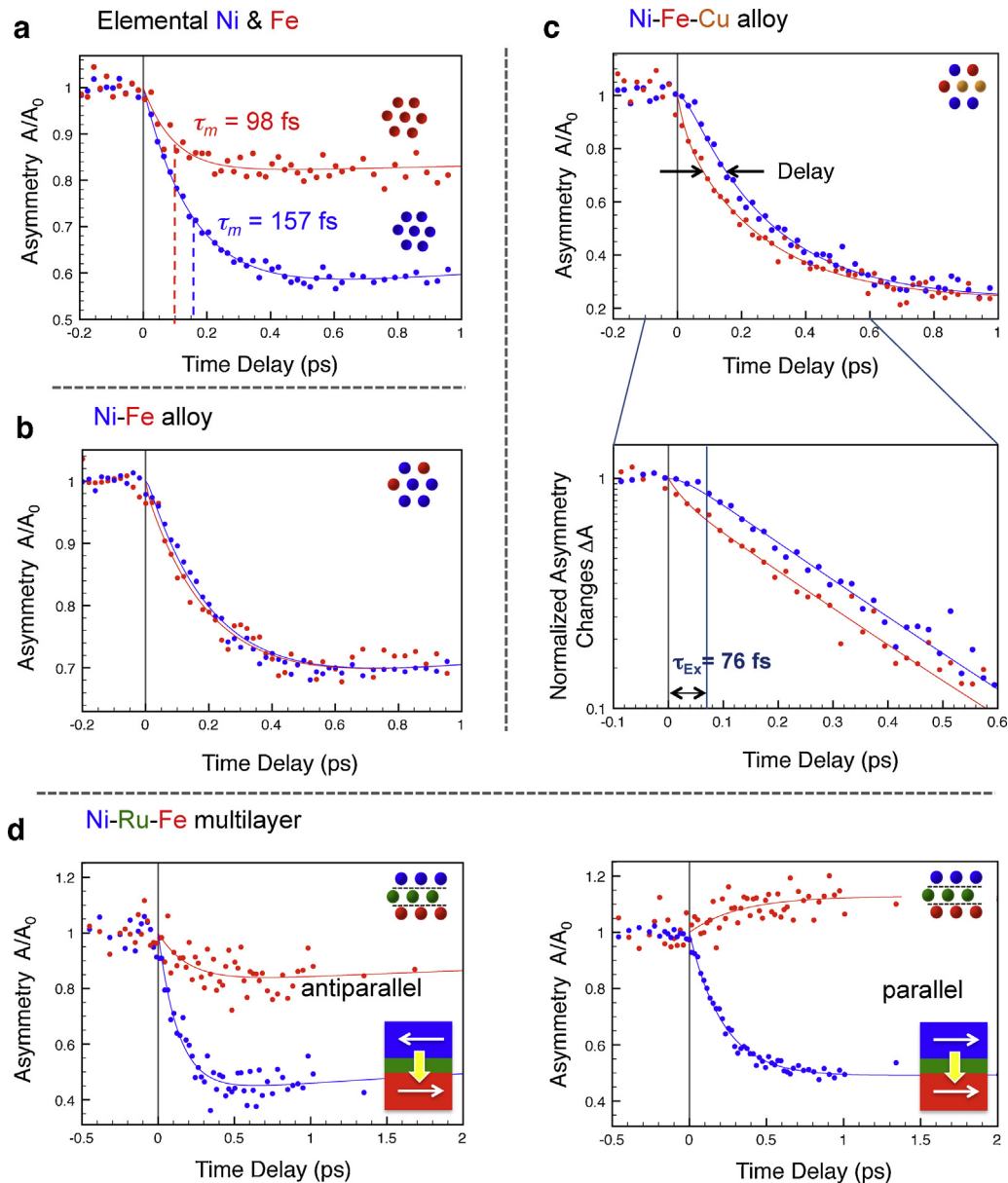


Fig. 6. From [15,16]. Ultrafast magnetization dynamics of Ni (blue dots) and Fe (red dots) in increasingly complex magnetic material systems. The dashed lines divide the graphs according to the different Ni and Fe compositions. After rapid excitation with a 780 nm, 1–2 mJ/cm², 25 fs pump pulse, the graphs show the magnetization dynamics of Ni and Fe as a function of pump-probe delay in: (a) elemental Ni and Fe, (b) Ni and Fe in Permalloy Ni₈₀Fe₂₀, (c) Ni and Fe in Permalloy (Py) alloyed with Cu (Py₆₀Cu₄₀), (d) and (e) Ni and Fe in a (Ni)-(1.5 nm Ru)-(Fe) trilayer stack. (For interpretation of the references to color in the artwork, the reader is referred to the web version of the article.)

can most impressively be demonstrated by a measurement of the ultrafast spin dynamics in the case where the magnetizations of the Ni and Fe layers are oriented parallel (Fig. 6e). Now, superdiffusion of majority spins from the Ni generates an ultrafast magnetization enhancement in the buried Fe layer by transiently increasing the number of the Fe majority spins. Our measurement therefore clearly shows the role of superdiffusive spin currents between different magnetic layers on femtosecond magnetization dynamics in complex multilayer stacks. The measurement additionally indicates that superdiffusive spin currents might add a substantial contribution to the heavily discussed “usual” ultrafast demagnetization process [2–13] that follows the optical excitation. A detailed analysis on the role of superdiffusive spin-currents in magnetization/demagnetization dynamics, that takes into account the competition between spin-flip scattering processes and spin diffusion, requires further measurements and theory. Such studies are underway. However, we demonstrate that a controlled

modification of the Fe and Ni environment together with an element-specific ultrafast probe opens up first experimental access to very important and typical correlated microscopic processes involved in femtosecond magnetization dynamics.

5. Conclusion

Ultrafast magnetization dynamics are a challenging area of science where the fundamental microscopic processes remain elusive, despite nearly two decades of research. New experimental capabilities need to be developed in order to disentangle the various physical processes and validate theoretical models, and in particular to enable the study of ultrafast magnetism in more complex and technologically relevant materials. We have shown here that a very promising way to overcome current experimental limitations is to use ultrashort X-ray pulses to explore ultrafast magnetic dynamics, which opens up the possibility of

studying magnetization dynamics with element-specificity and nanometer spatial resolution. High-harmonic upconversion of a table-top femtosecond laser enables element-specific, simultaneous, attosecond-to-femtosecond time-resolved measurements of the magnetic state with XUV T-MOKE. Making use of these new experimental capabilities, we elucidated the role of the exchange interaction on magnetization dynamics in alloys on ultrashort timescales. Furthermore, we isolated the contribution of superdiffusive spin currents in ultrafast magnetization processes in magnetic multilayer stacks, and used this effect to induce an increase of the magnetization in a buried Fe layer on femtosecond timescales.

Acknowledgments

Contribution of the National Institute of Standards and Technology, an agency of the U.S. government, not subject to U.S. copyright. The authors gratefully acknowledge funding from the U.S. Department of Energy Office of Basic Energy Sciences, Award #DE-FG02-09ER46652 and from the Deutsche Forschungsgemeinschaft, #Schn-353/17, #AE-19/20 and #GR 4234/1-1. S.M. was supported by the European Community's FP7 under Marie Curie International Outgoing Fellowship GA 253316. We also thank P.M. Oppeneer and M. Battiato (Uppsala University) for valuable discussions.

References

- [1] E. Beaurepaire, J. Merle, A. Daunois, *Phys. Rev. Lett.* 76 (1996) 4250.
- [2] A. Kirilyuk, A. Kimel, *Rev. Mod. Phys.* 82 (2010) 2731.
- [3] M. Cinchetti, M. Sánchez Albaneda, D. Hoffmann, T. Roth, J.-P. Wüstenberg, M. Krauß, O. Andreyev, H.C. Schneider, M. Bauer, M. Aeschlimann, *Phys. Rev. Lett.* 97 (2006) 177201.
- [4] B. Koopmans, G. Malinowski, F. Dalla Longa, D. Steiauf, M. Faehle, T. Roth, M. Cinchetti, M. Aeschlimann, *Nat. Mater.* 9 (2010) 259.
- [5] M. Krauss, T. Roth, S. Alebrand, D. Steil, M. Cinchetti, M. Aeschlimann, H.C. Schneider, *Phys. Rev. B* 80 (2009) 180407.
- [6] G. Zhang, W. Hübner, *Phys. Rev. Lett.* 85 (2000) 3025.
- [7] J.-Y. Bigot, M. Vohr, E. Beaurepaire, *Nat. Phys.* 5 (2009) 515.
- [8] M. Battiato, K. Carva, P.M. Oppeneer, *Phys. Rev. Lett.* 105 (2010) 027203.
- [9] K. Carva, M. Battiato, P. Oppeneer, *Phys. Rev. Lett.* 107 (2011) 207201.
- [10] A.B. Schmidt, M. Pickel, M. Donath, P. Buczek, A. Ernst, V.P. Zhukov, P.M. Echenique, L.M. Sandratskii, E.V. Chulkov, M. Weinelt, *Phys. Rev. Lett.* 105 (2010) 197401.
- [11] M. Sultan, U. Atxitia, A. Melnikov, O. Chubykalo-Fesenko, U. Bovensiepen, *Phys. Rev. B* 85 (2012).
- [12] B.Y. Mueller, T. Roth, M. Cinchetti, M. Aeschlimann, B. Rethfeld, *New J. Phys.* 13 (2011) 123010.
- [13] U. Atxitia, O. Chubykalo-Fesenko, J. Walowski, A. Mann, M. Muenzenberg, *Phys. Rev. B* 81 (2010) 174401.
- [14] G. Zhang, W. Hübner, *Appl. Phys. B Lasers O* 68 (1999) 495–499.
- [15] S. Mathias, C. La-O-Vorakiat, P. Grychtol, P. Granitzka, E. Turgut, J.M. Shaw, R. Adam, H.T. Nembach, M.E. Siemens, S. Eich, C.M. Schneider, T.J. Silva, M. Aeschlimann, M.M. Murnane, H.C. Kapteyn, *P. Natl. Acad. Sci. USA* 109 (2012) 4792.
- [16] D. Rudolf, C. La-O-Vorakiat, M. Battiato, R. Adam, J.M. Shaw, E. Turgut, P. Maldonado, S. Mathias, P. Grychtol, H.T. Nembach, T.J. Silva, M. Aeschlimann, H.C. Kapteyn, M.M. Murnane, C.M. Schneider, P.M. Oppeneer, *Nat. Commun.* 3 (2012) 1037.
- [17] I. Radu, K. Vahaplar, C. Stamm, T. Kachel, N. Pontius, H.A. Duerr, T.A. Ostler, J. Barker, R.F.L. Evans, R.W. Chantrell, A. Tsukamoto, A. Itoh, A. Kirilyuk, T. Rasing, A.V. Kimel, *Nature* 472 (2011) 205.
- [18] C. Stamm, T. Kachel, N. Pontius, R. Mitzner, T. Quast, K. Holldack, S. Khan, C. Lupulescu, E.F. Aziz, M. Wietstruk, H.A. Durr, W. Eberhardt, *Nat. Mater.* 6 (2007) 740.
- [19] B. Pfau, S. Schaffert, L.M.U. Iler, C. Gutt, A. Al-Shemmary, F.B.U. ttner, R. Delaunay, S.D.U. sterer, S. Flewett, R.F.O. mter, J. Geilhufe, E. Guehrs, C.M.G.U. nther, R. Hawaldar, M. Hille, N. Jaouen, A. Kobs, K. Li, J. Mohanty, H. Redlin, W.F. Schlottter, D. Stickler, R. Treusch, B. Vodungbo, M.K.A. ui, H.P. Oepen, J.L.U. ning, G.G.U. bel, S. Eisebitt, *Nat. Commun.* 3 (2012) 1100.
- [20] T. Wang, D. Zhu, B. Wu, C. Graves, S. Schaffert, T. Rander, L. Müller, B. Vodungbo, C. Baumier, D. Bernstein, B. Bräuer, V. Cros, S. de Jong, R. Delaunay, A. Fognini, R. Kukreja, S. Lee, V. López-Flores, J. Mohanty, B. Pfau, H. Popescu, M. Sacchi, A. Sardinha, F. Sirotti, P. Zeitoun, M. Messerschmidt, J. Turner, W. Schlottter, O. Hellwig, R. Mattana, N. Jaouen, F. Fortuna, Y. Acremann, C. Gutt, H. Dürr, E. Beaurepaire, C. Boeglin, S. Eisebitt, G. Grübel, J. Lüning, J. Stöhr, A. Scherz, *Phys. Rev. Lett.* 108 (2012) 267403.
- [21] C. La-O-Vorakiat, M. Siemens, M.M. Murnane, H.C. Kapteyn, S. Mathias, M. Aeschlimann, P. Grychtol, R. Adam, C.M. Schneider, J.M. Shaw, H. Nembach, T.J. Silva, *Phys. Rev. Lett.* 103 (2009) 257402.
- [22] C. La-O-Vorakiat, E. Turgut, C. Teale, H. Kapteyn, M. Murnane, S. Mathias, M. Aeschlimann, C. Schneider, J. Shaw, H. Nembach, T. Silva, *Phys. Rev. X* 2 (2012) 011005.
- [23] B. Vodungbo, J. Gautier, G. Lambert, A.B. Sardinha, M. Lozano, S. Sebban, M. Ducoussou, W. Boutu, K. Li, B. Tudou, M. Tortarolo, R. Hawaldar, R. Delaunay, V. López-Flores, J. Arabski, C. Boeglin, H. Merdji, P. Zeitoun, J. Lüning, *Nat. Commun.* 3 (2012) 999.
- [24] H. Kapteyn, M. Murnane, I. Christov, *Phys. Today* 58 (2005) 39.
- [25] A. Rundquist, *Science* 280 (1998) 1412.
- [26] T. Popmintchev, M.-C. Chen, A. Bahabad, M. Gerrity, P. Sidorenko, O. Cohen, I.P. Christov, M.M. Murnane, H.C. Kapteyn, *P. Natl. Acad. Sci. USA* 106 (2009) 10516.
- [27] T. Popmintchev, M.-C. Chen, P. Arpin, M.M. Murnane, H.C. Kapteyn, *Nat. Photon* 4 (2010) 822.
- [28] T. Popmintchev, M.-C. Chen, D. Popmintchev, P. Arpin, S. Brown, S. Alisauskas, G. Andriukaitis, T. Balciunas, O.D. Muecke, A. Pugzlys, A. Baltuska, B. Shim, S.E. Schrauth, A. Gaeta, C. Hernandez-Garcia, L. Plaja, A. Becker, A. Jaron-Becker, M.M. Murnane, H.C. Kapteyn, *Science* 336 (2012) 1287.
- [29] H. Vonesch, J.-Y. Bigot, *Phys. Rev. B* 85 (2012).
- [30] A. Melnikov, I. Rzdolski, T. Wehling, E. Papaioannou, V. Roddatis, P. Fumagalli, O. Aktsipetrov, A. Lichtenstein, U. Bovensiepen, *Phys. Rev. Lett.* 107 (2011) 076601.
- [31] M. Battiato, K. Carva, P. Oppeneer, *Phys. Rev. B* 86 (2012) 024404.
- [32] S. Essert, H. Schneider, *Phys. Rev. B* 84 (2011) 224405.
- [33] E. Carpena, E. Mancini, C. Dallera, M. Brenna, E. Puppini, S. de Silvestri, *Phys. Rev. B* 78 (2008) 174422.
- [34] L. Miaja-Avila, G. Saathoff, S. Mathias, J. Yin, C. La-o-vorakiat, M. Bauer, M. Aeschlimann, M.M. Murnane, H.C. Kapteyn, *Phys. Rev. Lett.* 101 (2008) 046101.
- [35] H. Hochst, D. Rioux, D. Zhao, D. Huber, *J. Appl. Phys.* 81 (1997) 5679.
- [36] H. Hochst, D. Rioux, D. Zhao, D. Huber, *J. Appl. Phys.* 81 (1997) 7584.
- [37] C.N. Afonso, A.R. Lagunas, F. Briones, S. Giron, *J. Magn. Magn. Mater.* 15/8 (1980) 833.
- [38] P. Grychtol, R. Adam, S. Valencia, S. Cramm, D.E. Buegler, C.M. Schneider, *Phys. Rev. B* 82 (2010) 054433.
- [39] S. Valencia, A. Kleibert, A. Gaupp, J. Ruzs, D. Legut, J. Bansmann, W. Gudat, P.M. Oppeneer, *Phys. Rev. Lett.* 104 (2010) 187401.
- [40] M. Hecker, P. Oppeneer, S. Valencia, H. Mertins, C. Schneider, *J. Electron Spectrosc.* 881 (2005) 144–147.
- [41] M. Pretorius, J. Friedrich, A. Ranck, M. Schroeder, J. Voss, V. Wedemeier, *Phys. Rev. B* 55 (1997) 14133.
- [42] P. Grychtol, R. Adam, A.M. Kaiser, S. Cramm, D.E. Buegler, C.M. Schneider, *J. Electron Spectrosc.* 184 (2011) 287.
- [43] R. Adam, P. Grychtol, S. Cramm, C.M. Schneider, *J. Electron Spectrosc.* 184 (2011) 291.
- [44] B. Koopmans, M. van Kampen, J. Kohlhepp, W. de Jonge, *Phys. Rev. Lett.* 85 (2000) 844.
- [45] L. Guidoni, E. Beaurepaire, J. Bigot, *Phys. Rev. Lett.* 89 (2002) 17401.
- [46] J. Bigot, L. Guidoni, E. Beaurepaire, P. Saeta, *Phys. Rev. Lett.* 93 (2004) 77401.
- [47] P. Oppeneer, A. Liebsch, *J. Phys. Condens. Mat.* 16 (2004) 5519.
- [48] G.P. Zhang, W. Hübner, G. Lefkidis, Y. Bai, T.F. George, *Nat. Phys.* 5 (2009) 499.
- [49] K. Carva, D. Legut, P.M. Oppeneer, *Epl: Europhys. Lett.* 86 (2009) 57002.
- [50] K. Carva, M. Battiato, P.M. Oppeneer, *Nat. Phys.* 7 (2011) 665.
- [51] A. Melnikov, I. Radu, U. Bovensiepen, O. Krupin, K. Starke, E. Matthias, M. Wolf, *Phys. Rev. Lett.* 91 (2003) 227403.
- [52] G. Malinowski, F.D. Longa, J.H.H. Rietjens, P.V. Paluskar, R. Huijink, H.J.M. Swagten, B. Koopmans, *Nat. Phys.* 4 (2008) 855.
- [53] V. Zhukov, E. Chulkov, P. Echenique, *Phys. Rev. B* 73 (2006) 125105.